A least squares procedure for the evaluation of multiple generalized stress intensity factors at 2D multimaterial corners by BEM.

A. Barroso, E. Graciani, V. Mantič, F. París
Group of Elasticity and Strength of Materials, School of Engineering, University of Seville, Spain.

Abstract. Detailed characterization of linear elastic stress states at corners and crack tips requires knowledge of the stress singularity orders, the characteristic angular functions and the generalized stress intensity factors (GSIF). Typically a high accuracy is found in the literature for the evaluation of the stress singularity orders and characteristic angular functions (numerically computed from analytical expressions in most cases). Nevertheless, GSIF values, evaluated by means of a numerical model using FEM or BEM and usually by postprocessing the results, are often reported with a lower level of confidence. A robust procedure is presented in this work for the evaluation of the GSIF at multimaterial corners. The procedure is based on a simple least squares technique involving stresses and/or displacements, computed by BEM, at the neighbourhood of the corner tip. A careful verification of the robustness and accuracy of the procedure using a few benchmark problems in the literature has been carried out. Applications of the procedure developed to the evaluation of GSIFs appearing at corners in metal-composite adhesive lap joints are presented.

Keywords: Stress intensity factor, linear elastic anisotropic material, multimaterial wedge, singularity analysis.

1.- Introduction

Problems having abrupt changes in geometry and/or material properties at some singular points solved under the assumptions of linear elasticity present unbounded stresses (referred to as stress singularities), see Wieghardt (1907), Williams (1952), Vasilopoulos (1988), Dempsey and Sinclair (1979, 1981), Sinclair (2004) and Paggi and Carpinteri (2008). Neighbourhood of such a point is usually referred to as corner, multimaterial corner if several materials meet at this point or also cross points if the singular point is located inside the domain. If the conditions for small scale yielding apply, the obtained singular elastic solution at a certain distance to the corner tip is representative of the real stress state. In this case, the linear elastic solution using a polar coordinate system (r,θ) centred at the corner tip, see Figure 1, admits, with the exception of some degenerate cases, a representation for the stresses σ_{ij} and displacements u_i by the following asymptotic series expansion, see Kondratev (1967), Costabel and Dauge (1993), Knees and Sändig (2006) and Barsuk (2010) for a rigorous mathematical justification:

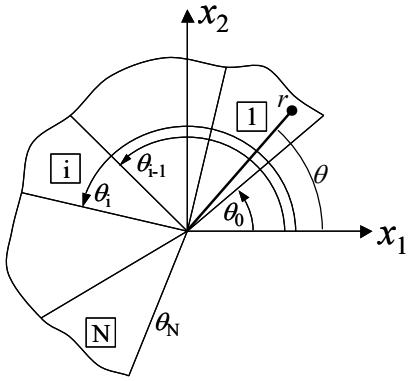

Fig. 1.- Multimaterial corner.

$$\sigma_{ij}(r,\theta) \cong \sum_{m=1}^{M} \frac{K_m}{r^{1-\lambda_m}} f_{ij}^m(\theta)$$
$$u_i(r,\theta) \cong \sum_{m=1}^{M} K_m r^{\lambda_m} g_i^m(\theta) \qquad , \qquad (i,j=r,\theta,z) \tag{1}$$

in which λ_m are the singularity exponents, $f_{ij}^m(\theta)$ and $g_i^m(\theta)$ are respectively the characteristic angular functions for stresses and displacements, and K_m, the weights of the terms, are the so-called Generalized Stress Intensity Factors (GSIF). Thus, the set of K_m (m=1,...,M) defines the local elastic state at a corner. Notice that each term in (1) represents a solution of the governing partial differential equations in the corner domain. We will refer to each term as a mode similar to that used in the case of cracks. It is assumed that λ_m are naturally ordered fulfilling Re $\lambda_m \le$ Re λ_{m+1}. Logarithmic terms have not been considered in this work for the sake of brevity; see Sinclair (1999) for further information. However, the procedure for the evaluation of GSIFs presented here may be easily generalized to include these logarithmic terms.

When a λ is a complex number, as in the case of interface cracks, $\lambda=\lambda_R+i\lambda_I$ (where λ_R and λ_I are real numbers), the associated GSIF is also a complex number $K=K_R+iK_I$ (where K_R and K_I are real numbers). In such a case, two terms can be included in (1). In the representation of the stresses, one term would be equal to K_R Re$\left[r^{\lambda-1} f_{ij}(\theta)\right]$ and the other would be K_I Im$\left[r^{\lambda-1} f_{ij}(\theta)\right]$, while in the representation of the displacements, one term would be equal to K_R Re$\left[r^{\lambda} g_i(\theta)\right]$ and the other K_I Im$\left[r^{\lambda} g_i(\theta)\right]$.

The characteristic angular functions $f_{ij}^m(\theta)$ and $g_i^m(\theta)$ together with the singularity exponents λ_m depend only on the local geometry, local material properties and the type of local boundary conditions. The GSIFs, K_m, in addition depend on the global geometry and prescribed boundary conditions, their values being proportional to the magnitude of boundary conditions for linear elastic solutions.

The rigid body motions are included in (1) for λ_m=0 (translations) and λ_m=1 (rotations) with the appropriate definition of g_i^m and the corresponding f_{ij}^m=0. Note that Re λ_m>0 for the other modes in (1).

The terms in (1) with Re δ_m>0, where δ_m =1-λ_m, thus 0<Reλ_m<1, are called singular, giving rise to unbounded stresses as $r\rightarrow 0_+$. In this case, δ_m are referred to as the stress singularity orders.

Failure predictions at these corner-points admit several approaches, most of them being based either on allowable values of these GSIFs or on allowable values of field variables evaluated by means of the local stress or strain fields governed by the GSIFs. The evaluation of these GSIFs is then of crucial importance. For the evaluation of the GSIFs, the global geometry and far field loading must be considered. Thus, in general, numerical models by means of FEM or BEM or experimental tests (e.g. using photoelasticity) have to be used. Techniques for the evaluation of GSIFs can be roughly divided into four basic groups, according to the local/global character of the procedure and to the necessity, or otherwise, of post-processing of the FEM or BEM analysis results.

Local techniques are sensitive to the accuracy of the numerical solution values for stresses and/or displacements close to the corner tip, while global techniques, working also, or only, with the elastic solution far from the corner tip, typically by making use of conservative integrals, are thus less sensitive to the solution accuracy at the corner tip. Regarding the second criterion for the classification, those techniques using postprocessing of basic field variables do not need to be incorporated into the numerical codes (FEM, BEM), but do not typically have as good accuracy as the methods which directly incorporate the singularity shape functions into the discretization, usually requiring a modification of the numerical code.

Some references belonging to these groups are included in Table 1, which do not aim to be an exhaustive review. Further information can be found in Helsing and Jonsson (2002a), Sinclair (2004) and Paggi and Carpinteri (2008). Particular examples of GSIF evaluation involving materials having non-isotropic constitutive laws can be found in Quaresimin and Ricotta (2006), Nomura *et al.* (2009) using the *H*-integral and including thermal stresses, or the interaction integral by Cisilino and Ortiz (2005).

	Local techniques	Global techniques
Evaluation of GSIFs using postprocessing of numerical (FEM, BEM) results	Based, e.g., on least squares adjustment (Chan *et a*l. 1970, Munz and Yang, 1993), Barroso *et al* (2004), Liu *et al* (2008).	Based, e.g., on conservative integrals, Banks-Sills (1997), Sinclair *et al* (1984), Omer & Yosibash (2005).
Incorporation of singularity shape functions in the problem discretization	Quarter point elements (Henshell & Shaw 1975, Barsoum 1976, Gray *et al*. 2003) and other singularity elements (Wait, 1978),	Functions in the whole domain (Helsing and Jonsson, 2002a) and (Marin, Lesnic and Mantič, 2004)

Table 1.- Classification of procedures for GSIF evaluation.

Typically, high accuracy can be found in the literature regarding the evaluation of singularity exponents λ_m and characteristic functions $f_{ij}^m(\theta)$ and $g_i^m(\theta)$ in (1), see Wieghardt (1907), Williams (1952) and Vasilopoulos (1988) for single isotropic corners, Dempsey and Sinclair (1979, 1981) for multimaterial isotropic corners, Mantič

(1997) for single orthotropic corners, Pageau *et al* (1995) for single anisotropic corners, Mantič *et al* (2003) for multimaterial anisotropic antiplane corners, Ting (1997), Barroso *et al* (2003), Hwu *et al.* (2003) and Yin (2003) for multimaterial anisotropic corners, which can be computed by finding the roots of an analytical function. However, the accuracy in the evaluation of GSIFs is substantially worse as numerical models of the global elastic problem and postprocessing of the results are needed. Reliable and accurate results for benchmark problems which could be used as reference values in new evaluation methods are needed. Some interesting comments regarding the validity of the published numerical results in the literature can be found in Helsing and Jonsson (2002b).

The approach proposed and explored in this paper is aimed at being an accurate and easy-to-use procedure for the evaluation of GSIFs. It can be located in the above classification in the first row (see Table 1), with no need to modify the FEM or BEM code applied, and between the two columns, as both near and far field data of the analysis results can be used. It should be noted that no special need for an accurate solution from the FEM or BEM analysis step in the neighbourhood of the corner tip is required, and it has a certain robustness with the use of the far-field data (far from the corner tip).

The paper is divided into five main sections. Section 2 deals with the description of the basic features of the Boundary Element code (BEM) applied, París and Cañas (1997) and Graciani *et al.* (2005), used for the numerical models in this work. Section 3 describes the postprocessing procedure for the evaluation of GSIFs, which is based on a least squares method in terms of the displacements and/or stresses using the results obtained along the boundary edges of the corner and also the common edges between material wedges in the case of a multimaterial corner. The proposed postprocessing procedure for evaluation of GSIFs K_m (m=1,...,M) is particularly well suited for numerical solutions arising from BEM models as the displacements and stress vector are the basic field variables used in the procedure. Nevertheless, no limitation appears in using the numerical solutions obtained by FEM models. Difficulties with the possible ill-conditioning of the resulting linear system are also analyzed in this section. Section 4 is devoted to the evaluation of the implemented procedure by means of the well known benchmark problems from the literature, performing parametric analyses to check the accuracy and robustness of the procedure. Section 5 applies the procedure for the evaluation of GSIFs in configurations of multimaterial corners appearing in adhesively bonded double-lap joints between aluminium and carbon fibre laminates. A final section summarizes the main features of the work.

2.- Main features of the multidomain BEM code

The present study involves the numerical analysis of 2D plane elasticity problems including one or multiple materials, with isotropic or orthotropic behaviours, in which singular stresses are present.

Two-dimensional BEM is employed in its traditional collocation formulation using continuous linear elements to mesh the boundaries of the problem in the displacement Somigliana identity.

The so-called displacement BIE can be obtained from the Somigliana identity by a well-known asymptotic analysis, París and Cañas (1997), Mantič and París (1995), Mantič and París (2004), yielding:

$$C_{ij}^K(\boldsymbol{x})u_j^K(\boldsymbol{x}) + \int_{\Gamma^K} T_{ij}^K(\boldsymbol{x},\boldsymbol{y})u_j^K(\boldsymbol{y})\,d\Gamma^K(\boldsymbol{y}) = \int_{\Gamma^K} U_{ij}^K(\boldsymbol{x},\boldsymbol{y})t_j^K(\boldsymbol{y})\,d\Gamma^K(\boldsymbol{y}) \qquad (2)$$

where $i,j = x,y$; $\boldsymbol{x}$ and $\boldsymbol{y}$ are, respectively, the collocation and integration points, both placed at the boundary Γ^K of the solid K under study; u_j^K and t_j^K are, respectively, the displacement and traction components; C_{ij}^K is the coefficient tensor of the free term; finally U_{ij}^K and T_{ij}^K are, respectively, the components of the fundamental solution in displacements and tractions. Superscript K is employed to denote the possibility of analyzing problems having multiple domains with possibly different linear elastic material behaviours.

The well-known analytic expressions of C_{ij}^K, U_{ij}^K and T_{ij}^K for isotropic materials can be found, for example, as in París and Cañas (1997). Simple explicit complex representations of U_{ij}^K and T_{ij}^K were introduced by Mantič and París (1995), along with a new analytical formula of the corresponding C_{ij}^K. Finally, explicit expressions of U_{ij}^K and T_{ij}^K for anisotropic mathematically non-degenerate and degenerate materials (i.e., with distinct and repeated roots of the sextic characteristic equation of the material) were presented in Mantič and París (2004).

In problems involving multiple materials, perfect bonding along the interfaces is assumed in the present work. The equilibrium and compatibility conditions are imposed using a weak formulation, see Blázquez *et al* (1998), Graciani *et al* (2005) and Blázquez *et al* (2006). This formulation permits the use of non-conforming boundary meshes along bonded boundaries. In such a case, although equilibrium and compatibility are not strictly imposed at the nodes of the boundary mesh, a smooth numerical solution is obtained which accurately fulfils the equilibrium and compatibility along the boundary in an average sense. Conversely, if conforming boundary meshes are employed (as in the examples presented in this paper), the use of the weak formulation of the equilibrium and compatibility conditions yields a system of equations which is a linear combination of the strong formulation of the equilibrium ($t_i^B + t_i^A = 0$) and compatibility ($u_i^B = u_i^A$) conditions at the nodes of the mesh of the bonded boundaries.

In some cases, depending on the local geometry and the boundary conditions, more than two unknowns may appear at certain nodes. In that case additional collocation equations are employed inside the elements adjacent to these nodes to ensure that a square matrix is obtained in the final system of equations, see París and Cañas (1997). If the boundary conditions permit the appearance of rigid body motions, the system of equations is appropriately modified by means of the *Method F2* described in Blázquez *et al* (1996), to obtain a non-singular square matrix in the final system of equations.

3.- Evaluation of the GSIFs

In the present work, the only unknowns which will be considered in the local asymptotic series expansion (1) are the GSIFs K_m (m=1,...,M). In the general procedure proposed and implemented by Barroso *et al* (2003), the analytic expressions of the characteristic angular functions are given in terms of the singularity exponents λ_m, which are computed as real or complex roots of an analytic function. A procedure based on a least squares method in terms of displacements and/or stresses will be described and studied in what follows to determine K_m.

The least squares method in displacements has been proved, Munz and Yang (1993), to be a simple and reliable method for the simultaneous evaluation of multiple GSIFs. In the present work, this approach has been extended to consider both displacements and/or stresses in order to evaluate the GSIF values. The present procedure, introduced by Barroso *et al* (2004) can also be considered a generalization of the work by Liu *et al.* (2008), as in the present proposal there is no limit to the number of stress singularities to be considered and these stress singularities, together with the characteristic angular functions, are obtained semi-analytically.

The proposed least squares fitting procedure is based on the minimization of the difference between the numerical solution (obtained by BEM in this work) and the analytical one (1), given in terms of unknown values of K_m (m=1,...,M). Hereinafter the BEM solution will be denoted by superscript "*BEM*" and the analytical one by superscript "*series*". The sum of squares of differences in values of the displacements, $u_\alpha^{series} - u_\alpha^{BEM}$, and tractions, $t_\alpha^{series} - t_\alpha^{BEM}$, at nodes placed along the radial edges of the corner are summed together. N_θ and N_r (see Figure 2) denote respectively the number of radial edges to be taken into account and the number of nodes taken at different distances along each radial edge. The so-called error function J, defined as

$$J(K_1,...,K_M) = aJ_u(K_1,...,K_M) + bJ_\sigma(K_1,...,K_M) \qquad (a,b \geq 0) \tag{3}$$

is built up with the contribution of the following sums of squares of differences in displacements J_u and the stress vector J_σ:

$$J_u(K_1,...,K_M) = \sum_{\alpha=r,\theta} \sum_{i=1}^{N_r} \sum_{j=1}^{N_\theta} a_\alpha \left[u_\alpha^{series}(r_i,\theta_j,K_1,...,K_M) - u_\alpha^{BEM}(r_i,\theta_j) \right]^2 \quad (a_\alpha \geq 0) \tag{4}$$

$$J_\sigma(K_1,...,K_M) = \sum_{\alpha=r,\theta} \sum_{i=1}^{N_r} \sum_{j=1}^{N_\theta} b_\alpha \left[t_\alpha^{series}(r_i,\theta_j,K_1,...,K_M) - t_\alpha^{BEM}(r_i,\theta_j) \right]^2 \quad (b_\alpha \geq 0) \tag{5}$$

The expression of J depends on the values of weights a and b, the usual choices being (a,b)=(0,1), (a,b)=(1,0) or (a,b)=(l^{-2},σ^{-2}) where l and σ are some characteristic length and stress values which make stresses and displacements have values of the same order of magnitude. The dimensionless weights a_α and b_α allow the isolated components of the nodal displacements and tractions to be used.

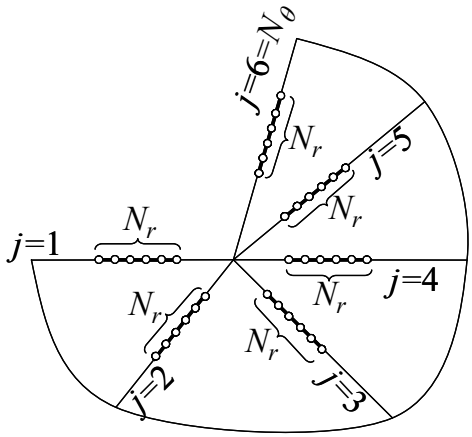

Fig. 2.- Definition of parameters used in the least squares procedure.

The use of BEM is particularly suitable for the evaluation of the error function J as the numerical results can be computed for the nodes defining the mesh. Nevertheless, no additional difficulty appears for the generalization of the error function J when working with an arbitrary set of nodes at any location inside a corner neighbourhood, a situation which will be useful in the case of having FEM results.

A set of GSIFs K_m (m=1,...,M) which minimizes the error function J in (3) is obtained by solving the following linear system of equations:

$$\frac{\partial J(K_1,...,K_M)}{\partial K_j} = 0 \quad (j=1,...,M) \tag{6}$$

The procedure admits complex values of the GSIFs, as detailed in Section 1. In such a case, two terms have to be included in (1) and correspondingly, two terms, associated to the real and imaginary parts of the GSIFs, have also to be taken into account in (6).

Note that additional data could be obtained from the BEM results at some internal points in the domain. However, the idea herein is to carry out an additional check of the procedure by trying to represent the stresses and displacements inside the corner neighbourhood domain using only BEM results at the boundary mesh nodes in the fitting process. This will give confidence in the overall process, as no domain data have been used to fit domain variables.

The resulting linear system arising from (6) will be calculated explicitly in the following. Only the displacement component u_r will be considered in the evaluation of the error function J (i.e. a_r=1, a_θ=0, a=1, b=0), for the sake of simplicity. The displacement u_r at a point (usually a node) n defined by the radius r_i and polar angle θ_j using M terms in the asymptotic series expansion representation (1) can be expressed by:

$$u_r^{series}(r_i,\theta_j) \cong \sum_{m=1}^{M} K_m r_i^{\lambda_m} g_r^m(\theta_j) = \sum_{m=1}^{M} a_{nm} K_m \tag{7}$$

where $a_{nm} = r_i^{\lambda_m} g_r^m(\theta_j)$ is the coefficient associated to the K_m-term of the series expansion of u_r in (1) evaluated at the point n with the polar coordinates (r_i,θ_j).

The derivative with respect to K_j of the error function J built with the displacement component u_r evaluated at N nodes (n=1,...,N) is a linear function of K_j (j=1,...M) which can be expressed as follows:

$$\frac{\partial J}{\partial K_j} = 2\sum_{n=1}^{N}\left\{\sum_{m=1}^{M} a_{nm}K_m - u_r^{BEM}(n)\right\}a_{nj} = 2\sum_{n=1}^{N}\left\{\sum_{m=1}^{M} a_{nm}K_m a_{nj} - a_{nj}u_r^{BEM}(n)\right\} = 0 \qquad (8)$$

where $u_r^{BEM}(n) = u_r^{BEM}(r_i,\theta_j)$ denotes the value of displacement u_r at the point n, usually coinciding (as mentioned previously) with a boundary element node. Expression (8) can be written in matrix notation as:

$$\mathbf{A}^T\cdot\mathbf{A}\cdot\mathbf{K} = \mathbf{A}^T\cdot\mathbf{b} \qquad (9)$$

where $\mathbf{A}$ is a (N×M) matrix, N and M being respectively the number of points (nodes) taken for building the error function J and M the number of terms in the series expansion (the number of GSIF values) (1). As long as the number of nodes N is greater than the number of terms considered for the displacement representation M, $\mathbf{A}$ is a rectangular matrix with more rows than columns and thus expected to have full rank M. $\mathbf{K}$ (M×1) is the vector of unknowns (GSIF values) and $\mathbf{b}$ (N×1) is the vector of numerical results for u_r at the chosen points.

$$\mathbf{A} = \begin{bmatrix} a_{11} & \cdots & a_{1M} \\ \vdots & & \vdots \\ a_{N1} & \cdots & a_{NM} \end{bmatrix},\ \mathbf{K} = \begin{bmatrix} K_1 \\ \vdots \\ K_M \end{bmatrix},\ \mathbf{b} = \begin{bmatrix} b_1 \\ \vdots \\ b_N \end{bmatrix} \qquad (10)$$

It is clear that the square (M×M) matrix $\mathbf{A}^T\cdot\mathbf{A}$ can have rank=M if and only if the number of nodes N is equal to or greater than the number M of GSIFs to be calculated. Only in that case can the inverse of $\mathbf{A}^T\cdot\mathbf{A}$ exist and be computed.

Equation (9) is the typical matrix expression that appears when solving an overdetermined linear system

$$\mathbf{A}\cdot\mathbf{K} = \mathbf{b} \qquad (11)$$

using the 2-norm minimization $\min_{\mathbf{K}}\left\|\mathbf{A}\cdot\mathbf{K}-\mathbf{b}\right\|_2$, see Golub and van Loan (1996) or Trefethen and Bau (1997). Notice that the fulfilment of (11) corresponds to the vanishing differences in the error function J, i.e. J=0.

The solution $\mathbf{b}$ of the full rank least squares problem is theoretically unique. Nevertheless, due to the nature of the matrix components $a_{nm} = r_i^{\lambda_m} g_r^m(\theta_j)$, the evaluation of the matrix $\mathbf{A}^T\cdot\mathbf{A}$ using only nodes very close to the corner tip has been shown to give rise to ill-conditioned matrices with numerically computed rank($\mathbf{A}^T\cdot\mathbf{A}$)<$M$. This ill-conditioning includes the cases in which the number of nodes N

exceeds the number of GSIF terms M and the matrix $\mathbf{A}$ has numerically computed full rank M. The conditioning number for the 2-matrix norm (see, for example, Golub and van Loan, 1996, Trefethen and Bau, 1997) $\kappa(\mathbf{A}) = \|\mathbf{A}\|_2 \left\|\mathbf{A}^+\right\|_2 = \sigma_{\max} / \sigma_{\min}$, where $\mathbf{A}^+$ is the pseudoinverse of $\mathbf{A}$, and $\sigma_{\max}$ and $\sigma_{\min}$, respectively, are the maximum and minimum singular values of $\mathbf{A}$, gives an indication of the conditioning of the problem. It has been numerically verified, for example, in the problem of Section 4.2 that $\kappa(\mathbf{A})$ in these cases (in which the number of nodes N exceeds only slightly the number of GSIF terms M) is around 10^3 times higher than the conditioning number obtained in those cases where the number of nodes N is much greater than the number of GSIF terms M.

Also the relative proximity between the nodes chosen for the evaluation of the error function J or, equivalently, matrix $\mathbf{A}$ has been shown to affect the numerical conditioning of $\mathbf{A}^T \cdot \mathbf{A}$. When consecutive nodes are chosen for the evaluation of J, the number of nodes needed for $\mathbf{A}^T \cdot \mathbf{A}$ to have numerically computed full rank has been shown to be significantly greater than when non-consecutive nodes are chosen.

Taking all these considerations into account, the least squares solution has been computed in the present work, solving system (11) directly by means of the **QR** decomposition of matrix $\mathbf{A}$, which is known to be more accurate than directly solving the system in (9) with a possibly ill-conditioned matrix $\mathbf{A}^T \cdot \mathbf{A}$.

The extension of the proposed procedure to 3D problem is straightforward. Provided that 3D asymptotic series expansion for the displacement and stress representation is available for the corresponding 3D problem under analysis, the procedure needs minor changes to take into account the new asymptotic series expansion of stress and displacement at the 3D corners and the usage of nodes of a 3D mesh.

4.- Computation of GSIFs for benchmark problems

The evaluation of the accuracy of the procedure described in Section 3 and implemented in a BEM code is quite independent of the complexity of the global elastic problem, as it is based on the evaluation of displacements and/or stresses at a certain set of points close to the corner tip. A preliminary check of the accuracy exclusively due to the procedure and to the numerical model has been performed in the first benchmark problem (Section 4.1) with boundary conditions which reproduce either single pure mode I and/or single pure mode II loading. These conditions are imposed as external loading at the boundary, taking only the first term of mode I and/or mode II of the corresponding series expansion (1). Thus, this problem does not really represent global boundary effects, the solution in the entire domain being given by single pure mode I and/or single pure mode II solution from series (1).

A second benchmark problem (Section 4.2) corresponding to a 90º notch subjected to a tensile loading has also been analyzed. This is a classical problem with an accurate solution up to the tenth digit presented in Helsing and Jonsson (2002a). We will use this problem to see the boundary effects and their influence on the approximate least squares solution.

These two benchmark problems have only free edges converging to the corner tip, the only option in the present BEM formulation being to use displacement components in the evaluation of the error function (3-5) (i.e. b=0).

A third benchmark problem (Section 4.3) is a bimaterial (isotropic-isotropic) free-free corner subjected to tensile loading.

Comparison with previously published works is, in many cases, not a straightforward task due to the lack of information regarding characteristic angular functions, the standardization methods adopted to normalize GSIF values and/or explicit expressions of the analytical solution (if available). Note that the absolute values of GSIFs are dependent on the expression of the characteristic angular functions as stressed by Pageau *et al*. (1996), Hwu and Kuo (2007), and Song *et al* (2010).

4.1.- Pure and mixed singular mode problems

Let us consider the geometry, shown in Fig. 3, containing a 90º notch with h/w=1 and d/w=0.5. The analytical solution for the first singular term of the series expansion in (1) corresponding to the symmetric mode I, λ_I=0.544483736782, or the second singular term corresponding to the skew-symmetric mode II, λ_{II}=0.908529189846, or both for a mixed mode, has been imposed along the boundary as the external loading. It has to be pointed out that the global geometry does not play a relevant role in this particular problem. The only relevant geometrical feature is the internal angle associated to the straight edges emanating from the corner tip, which define the corner geometry, since the same solution applied to any other arbitrary geometry (having an internal 90º notch) would give rise, basically, to the same results (although there can be some influence of the global geometry on the BEM numerical solution of the problem). The rigid body displacements have been removed by subtracting from all the displacement values at the chosen points the displacement values at the corner tip (this makes the corner tip fixed, i.e. u_x=u_y=0) and the rotation was set free and included in the u_θ component by means of the term $K_r \cdot r$, λ_r=1. Further information about rigid body effects can be found at Blázquez *et al* (1996).

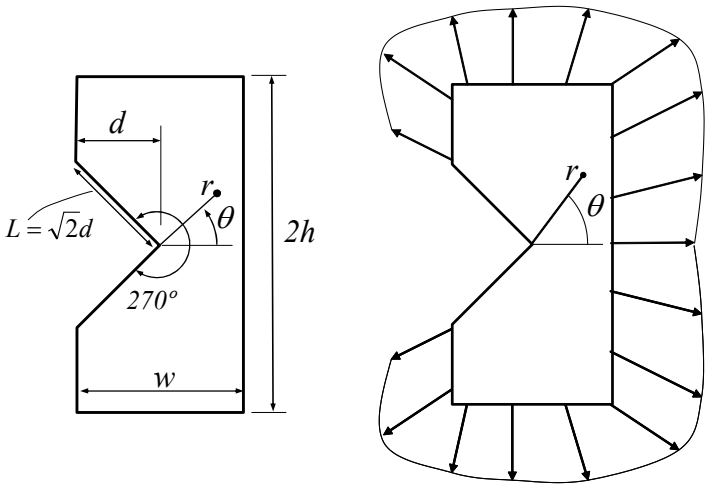

Fig. 3.- Free-free corner problem. a) geometry, b) tractions of the pure singular mode-I.

The stresses and displacements for pure singular mode I and mode II are explicitly known (see, for example, Vasilopoulos, 1988).

Taking w=10 mm (and then: d=5 mm and h=10 mm), a BEM model was built with 709 nodes, using continuous linear elements 0.1 mm in size along the horizontal and vertical faces while along the inclined faces a progressive geometric refinement (with a ratio of 1.5 between the length of consecutive elements) towards the corner is applied up to an element size of 10^{-8} mm. The distance between consecutive nodes grows geometrically up to node number 40 (r=0.22 mm from the corner tip), and then a uniform mesh is used with an element size of 0.1mm. In this way, each inclined face has a total of 100 nodes. The three combinations of mode I and mode II solutions shown in Table 2 have been analyzed, the first two corresponding to pure modes and the third to a mixed mode.

Mode I (symmetric)	Mode II (skew-symmetric)	Mixed mode
K_I=1	K_I=0	K_I=0.6
K_{II}=0	K_{II}=1	K_{II}=0.9

Table 2.- Pure and mixed singular mode loading cases for the 90º notch problem.

In this simple problem, only displacements (u_r and u_θ) have been used for the evaluation of the error function J in (3), due to the vanishing of the stress vector at the edges $\theta=\alpha=\pm 135º$. This is equivalent to taking a=1 and b=0 in (3). Due to the loading cases under consideration, only the numerical results along one edge (N_θ=1) will be taken into account as the results along the other edge will be symmetric (mode I), skew-symmetric (mode II) or a combination of both in the mixed mode, with no additional information added in any case.

The number of points (N_r) along a straight corner edge to be used in the determination of K_k is a significant parameter in the evaluation of J in (3). Thus, all possible combinations of consecutive nodes have been considered analyzing their influence on the accuracy of the results. In the three cases studied analogous results were found, with very satisfactory results (values for K_I and K_{II} very close to those defining the prescribed boundary tractions in Table 2) with the exception of a few small groups of nodes located very close to the corner tip. As the applied boundary conditions are the analytical solutions for the stresses, no lack of accuracy appears when using a small group of nodes far away from the corner tip in the least squares procedure. These effects will be clearly observed in the next section where a tensile loading is applied instead of the pure singular mode loading.

The influence of considering only one or both displacement components can be observed in Table 3, in which a fixed group of nodes is always used: with distances to the corner tip of between 10^{-6} mm and 0.33 mm (the length of the edge $\theta=\alpha=\pm 135º$ is $5\sqrt{2}$ =7.07 mm), avoiding the nodes closest to the corner tip. In Table 3 the word *rotation* means that u_θ includes the rigid body rotation term ($K_r \cdot r$).

	Components used in the procedure	K_I	Error K_I (%)	K_{II}	Error K_{II} (%)	K_r (rotation)
Mode I	u_r	0.994712	0.53	0.002266	-	-
K_I=1	u_θ	0.991847	0.82	0.000951	-	-
K_{II}=0	u_θ (+ rotation)	0.986735	1.33	0.006987	-	$1.6\ 10^{-8}$

Mode II	u_r	-0.001729	-	1.000040	0.004	-
K_I=0	u_θ	-0.709667	-	0.161691	83.83	-
K_{II}=1	u_θ (+ rotation)	0.001148	-	1.000950	0.095	$2.2\ 10^{-6}$
Mixed	u_r	0.595270	0.47	0.901396	0.14	-
mode	u_θ	0.043592	55.64	0.144951	75.50	-
K_I=0.6	u_θ (+ rotation)	0.593074	0.69	0.896664	0.33	$2.0\ 10^{-6}$
K_{II}=0.9	u_r+u_θ (+ rotation)	0.598593	0.35	0.900840	0.08	$2.0\ 10^{-6}$

Table 3.- Results in pure mode loadings.

In all three cases a search was carried out for the unknown values of K_I, K_{II} and K_r. All cases show very good accuracy (below 1%) except those cases where rigid body rotation appears and is not considered in the evaluation of J (3). In mode I loading, if the rotation term K_r is considered (without real rotation in the model, due to the symmetry) an additional null term (associated to the value of K_r) is artificially included in the procedure and the error in K_I increases, although it is still reasonably low from an engineering point of view (1.33 %).

In those loading cases with rigid body rotation, it is mandatory to search for K_r if u_θ is used in the least squares procedure. Nevertheless, as the rigid body rotation only affects the u_θ component, if only u_r is included in the evaluation of J (3) the accuracy will obviously not be influenced by including K_r.

In the mixed mode loading (K_I=0.6 and K_{II}=0.9) the same trends are observed and excellent results from an engineering point of view (<1%) can be expected if all possible terms (K_I, K_{II} and K_r) are included. The best results are observed when both (u_r and u_θ) are included for the error evaluation (0.35% for K_I and 0.08% for K_{II}).

4.2.- The 90º notch subjected to tensile loading

Once the accuracy of the procedure has been checked in single pure and mixed singular mode problems where the outer boundaries are irrelevant (as we particularized the asymptotic solution, with one or two singular terms in (1), along these boundaries), problems in which the asymptotic series expansion is only valid at some neighbourhood of the corner tip will be now analyzed. Considering the same geometry as in the previous problems, now the loading condition is given by a uniform normal traction at the upper and lower edges which generates a mode I symmetric solution at the neighbourhood of the corner tip.

This benchmark problem, depicted in Fig. 4, has been taken from Helsing and Jonsson (2002a), where several results from previous works are also included and the result for K_I with an accuracy up to 13 digits is reported, K_I=4.295886967699. The present procedure allows the rigid body displacements to be restricted at any points, but taking into account that finally the relative displacements with respect to the corner tip (the corner tip being fixed, i.e. u_x=u_y=0) are used in the least squares fitting.

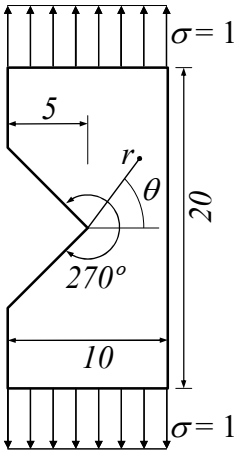

Fig. 4.- The 90º notch subjected to tensile loading (Helsing and Jonsson, 2002a).

In this problem the same approach as used in Section 4.1 has been adopted. Thus, the same boundary element mesh, the same values for a=1 and b=0 in the expression of J (3), and also u_r and/or u_θ components of the displacements have been used for the evaluation of J (3).

All possible combinations of groups of consecutive nodes (with 100 nodes per edge, a total of (100x100)/2=5000 combinations appear) have been analyzed for the evaluation of J. Using BEM models, direct results for displacements and stress vector components are obtained at nodes placed along the domain boundary.

The results (errors in % for K_I value) are presented in Fig. 5. Figure 5 has 6 plots, couples of plots (a,b), (c,d) and (e,f) correspond to results considering, respectively, M=3, 5 and 7 terms of the series expansion in (1), using displacements u_r and u_θ in the expression of the error function J (3). The plots show the same results taking into account the node distance (Figures 5a, c and e) or the node number (Figures 5b, d and f). The number of terms used corresponds to the following relations for singular exponents: $0<\lambda_1$ and $\lambda_2<1$ (singular modes), $\lambda_3=\lambda_r$ (rigid body rotation mode), $\lambda_4=\overline{\lambda_5}$ and $\lambda_6=\overline{\lambda_7}$ (complex conjugated regular modes).

In problems where an accurate result is not available, the regression coefficient R^2 is a good parameter to estimate the accuracy of the fitting procedure.

Plots in Fig. 5 present at the right and left axes, respectively, the initial and final distance of the selected group of nodes (Figures 5a, c and e) or initial and final node numbers (Figures 5b, d and f), with node numbering starting at the corner tip, taken along the inclined edges with a total length of $5\sqrt{2}$=7.07 mm (or 100 nodes), and the vertical axis, the error in K_I (in %), which has been plotted truncated at a 5% for the sake of clarity in the graphical representation (errors higher than a 5% have been represented as a flat surface at 5% error, this makes the representation of the surface with errors below 5% clearer and more readable). The upper half-part of the figures is meaningless in all plots.

Plots in Figure 5 clearly show the importance of a suitable choice of the group of nodes selected to perform the least squares adjustment. With a graphical representation like the one in Figure 5, a group of nodes in the flattest zone of the non-truncated error surfaces should be chosen to evaluate K_I (remind that the flat zone of the top part of the

error surface, in Figure 5, are not really flat and just represents errors higher than a 5%). Groups of nodes close to the large slopes of the figures should be avoided. In other proposals (e.g. Liu *et al*, 2008) this choice is made by finding the group of nodes that best adjusts the stress singularity orders (which, thus, have to be known *a priori*).

Due to the fact that the node distances to the corner tip grow geometrically in a neighbourhood of the corner tip (up to node number 40) and then a uniform mesh is used, both representations (distances, at the left hand side, or nodes, at the right hand side) show a different aspect of the error surface. Notice that the node number in Figures 5b, d and f is proportional to the log(distance), up to node number 40.

In the representation using distances to the corner tip (Figures 5a, c and e) it can be observed that for initial node distance lower than a particular value (for example, in Figure 5e around 4 mm) all groups of nodes yield reasonably low errors. In the representation using node numbers (Figures 5a, c and e), it can additionally be observed that groups of nodes close to the corner tip should also be avoided. When using a refined mesh, as it is the case in this analysis, avoiding a few nodes at the corner tip is enough to achieve good results from an engineering point of view. For example, to avoid the errors shown at the right hand side of Figures 5b, 5d and 5f, do not use any group of nodes between 0 and 20 to get errors below 4%, between 0 and 30 to get errors below 3%, etc.

Thus, small groups of nodes too far from or too close to the notch tip yield higher errors of K_I. The more terms taken into consideration in the series expansion (1), the lower the errors to be found at higher distances from the notch tip. Additionally, the groups of nodes having only a few more nodes than the number of GSIF terms under consideration, i.e. $N\tau M$, show higher values of the error, as the resulting linear system is very ill-conditioned.

In fact, as mentioned previously, in Section 3, at least the same number of nodes (N) as the number (M) of K_m being included in (1) and (3) is strictly necessary to make the linear system non-singular (the coefficient matrix has full rank), i.e. $N \geq M$. In Figure 5, at least, $N=M+1$ nodes have been considered for the fitting procedure in all plots.

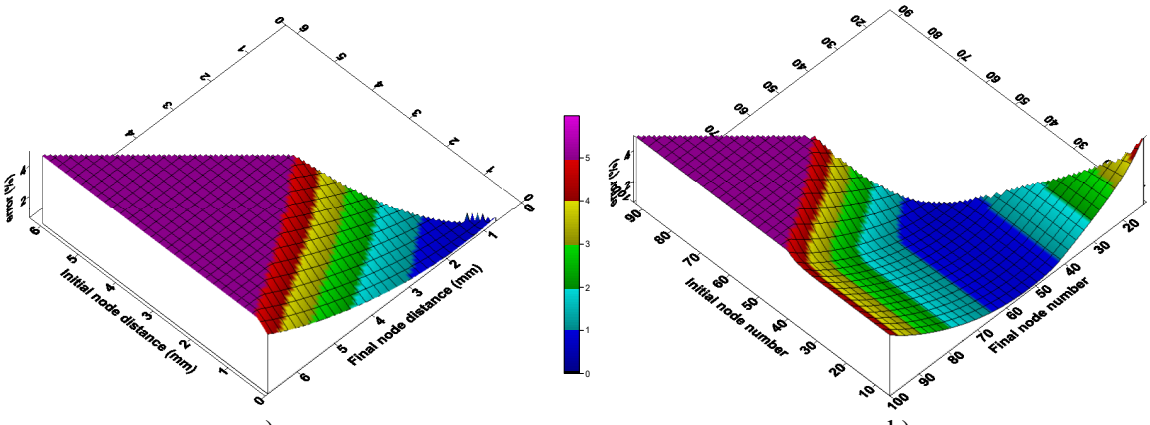

a) b)

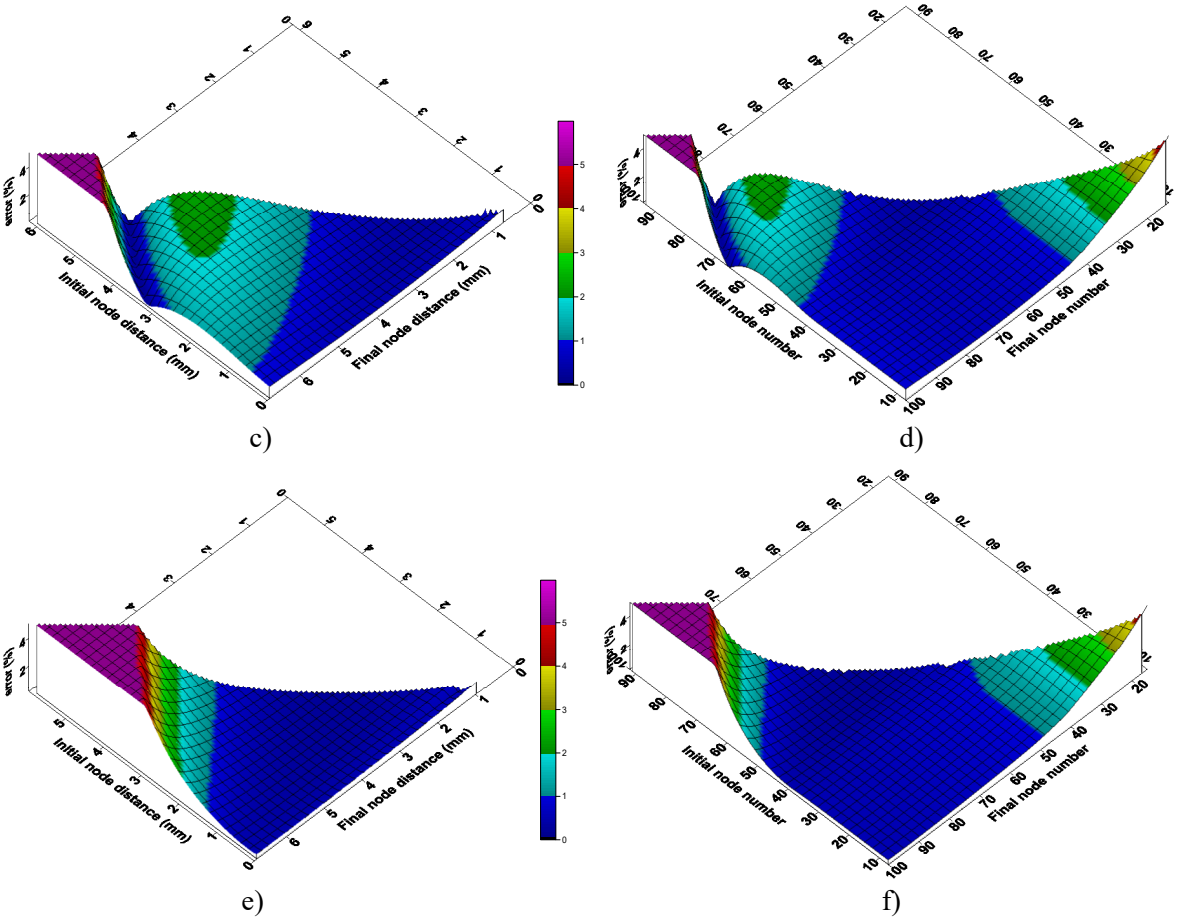

Fig. 5.- Errors in K_I considering: a-b) M=3, c-d) M=5 and e-f) M=7 terms in the series expansion (1), a), c) and d) pictures including node distances and b), d) and f) including node numbers.

With reference to the influence of the terms of the series expansion used, in general, the higher the number of terms (M), the lower the error found. Acceptable results (errors <1%) are found in most of the reasonable groups of nodes, avoiding small groups ($N\tau M$) far away from the notch tip.

In view of the error distributions in Figures 5a, c and e it seems that the variation of error for groups of nodes with approximately the same position of the central point (the arithmetic mean of the largest and smallest distances of nodes in the group, respectively, r_{max} and r_{min}, to the corner point), $r_c=(r_{max}+r_{min})/2$, is relatively small.

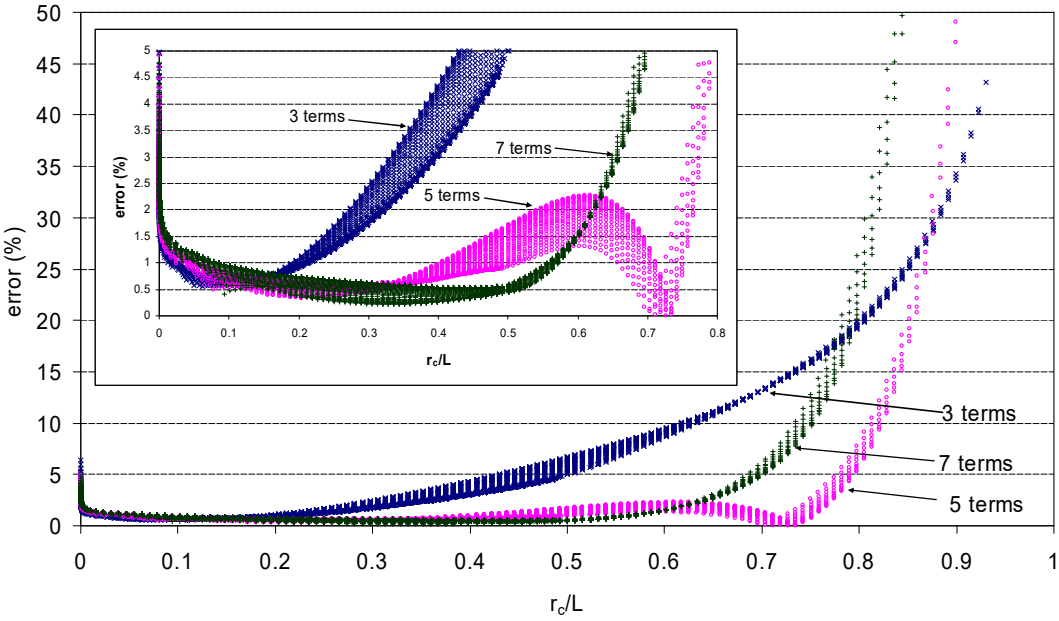

Fig. 6.- Errors in K_I considering M=3, 5 and 7 terms as a function of r_c/L.

This observation has motivated the representation in Figure 6, where the error is plotted for all groups of nodes considered in Figures 5 as a function of the central point distance to the corner tip r_c. These plots confirm that r_c/L is a very relevant parameter and that for small M, a suitable r_c/L should be relatively small, while for larger M values r_c/L can be larger. In particular, in the present problem the optimal values of r_c/L are around 0.1, 0.2 and 0.3~0.4, respectively, for M=3, 5 and 7. In general, groups of nodes with r_c/L>0.5 are not suitable for K_I evaluation in this problem.

4.3.- The isotropic free-free bimaterial corner.

The problem, depicted in Fig. 7, of an isotropic free-free bimaterial corner subjected to tensile loading has been taken from Qian and Akisanya (1999), a configuration which was analyzed later by Ortiz *et al* (2005) and Alcalá (2008). This problem is still simple enough to have a relatively simple analytic solution of the asymptotic field of stresses and displacements in terms of λ_m and K_m.

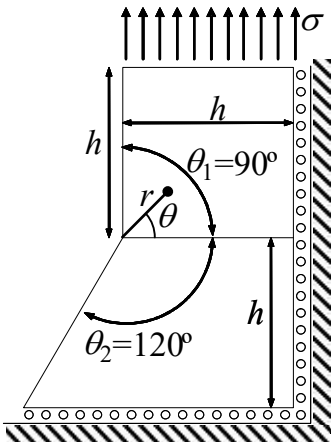

Fig. 7.- Bimaterial free-free isotropic corner (Qian and Akisanya, 1999).

Qian and Akisanya reported results for the following Dundurs parameters: α=0.8 and β=0.2, which correspond to a system in which the upper material is about ten times stiffer than the lower material. The expressions for displacements and stresses by Qian and Akisanya (using their nomenclature) are:

$$\sigma_{ij}^{m}(r,\theta)=\sum_{k=1}^{N}H_k r^{\lambda_k-1} f_{ijk}^{m}(\theta)\,,\quad u_i^{m}(r,\theta)=\sum_{k=1}^{N}H_k r^{\lambda_k} g_{ik}^{m}(\theta) \tag{12}$$

where

$$H_k=\sigma h^{1-\lambda_k} a_k(\alpha,\beta,\lambda_k,\theta_1,\theta_2)\,. \tag{13}$$

In (12-13) m is the material, H_k is the GSIF associated to the corresponding λ_k, a_k is the dimensionless GSIFs (equal to H_k when h=1 mm and σ=1 MPa), $f_{ijk}^{m}(\theta)$ and $g_{ik}^{m}(\theta)$ are known characteristic angular functions, see Qian and Akisanya (1999), α and β are the Dundurs parameters and θ_1 and θ_2 are the solid angles for both solids (90º and 120º respectively in the present case).

The corner in Figure 7 has only one singular mode ($0<\lambda_1<1$), Qian and Akisanya reporting the first three singularity exponents: λ_1=0.6747, λ_2=1.1637 and λ_3=1.5938. These values are in relatively good agreement with those obtained using the analytical procedure (including a numerical computation of roots of an analytic function) by Barroso *et al.* (2003): λ_1=0.673473 (0.18% difference), λ_2=1.167477 (0.32% difference) and λ_3=1.589147 (0.29% difference).

The GSIF values obtained by Qian and Akisanya using FEM and by means of a path-independent contour integral (finally transformed into a domain integral) effectively show a reasonable path independency when evaluated at different distances from the corner tip: 0.0053h-0.0063h, 0.0217h-0.0255h and 0.0869h-0.11h as shown in Table 4. The average values and variation coefficients reported for the three domains are respectively a_1=0.6301 (VC=0.009%), a_2=-0.3671 (VC=0.129%) and a_3=0.5443 (VC=0.798%).

	r=0.0053h-0.0063h	r=0.0217h-0.0255h	r=0.0869h-0.11h	average
a_1	0.6301	0.6301	0.6300	0.6301
a_2	-0.3666	-0.3673	-0.3675	-0.3671
a_3	0.5407	0.5430	0.5491	0.5443

Table. 4.- Results for a_1, a_2 and a_3, by Qian and Akisanya (1999).

This problem has also been analyzed, using other techniques, by Ortiz et al (2005) and Alcalá (2008). A summary of their results is presented prior to the present results. The idea is to compare all of them, as each one uses a different approach to evaluate the GSIFs.

Ortiz *et al*. (2005) reported for the same configuration, and using a domain-independent integral in conjunction with a 3D BEM model considering plane strain boundary

conditions, the values for a_1 and a_2 shown in Table 5 (where z/t is the relative depth and r/h the radial distance to the notch). The average values and variation coefficients are a_1 =0.67829 (VC=0.16%) and a_2 =-1.54431 (VC=1.44%).

		z/t=0.0	z/t=0.5	z/t=1.0	average
a_1	r/h=0.2	0.67700	0.67697	0.67669	0.67829
	r/h=0.3	0.67877	0.67876	0.67853	
	r/h=0.4	0.67938	0.67938	0.67918	

a_2	r/h=0.2	-1.52424	-1.51860	-1.50673	-1.54431
	r/h=0.3	-1.55476	-1.55223	-1.54716	
	r/h=0.4	-1.56654	-1.56558	-1.56294	

Table. 5.- Results for a_1 and a_2 by Ortiz *et al*. (2005).

Alcalá (2008) also analyzed the same problem, using the *H*-integral, see Bueckner (1973), with a 2D BEM model, the values for a_i (i=1,2,3) being evaluated at the same distances from the corner tip as used by Qian and Akisanya. The results, in Table 6, show average values for a_1=0.6788 (VC=0.075%), a_2=-1.538 (VC=2.62%) and a_3=0.5630 (VC=60.7%) or a_3=0.7732 (VC=3.6%), eliminating the first two results for a_3 (at r=0.0053h and r=0.0063h), which do not show the uniformity of the other four results.

	r=0.0053h	r=0.0063h	r=0.0217h	r=0.0255h	r=0.0869h	r=0.11h	average
a_1	0.6784	0.6781	0.6788	0.6788	0.6795	0.6792	0.6788
a_2	-1.4746	-1.5006	-1.5585	-1.5581	-1.5686	-1.5683	-1.538
a_3	-0.0174	0.3026	0.7553	0.7433	0.7942	0.7999	0.7732

Table. 6.- Results for a_1, a_2 and a_3, by Alcalá (2008).

Results from Qian and Akisanya, Ortiz and Alcalá will be compared with those obtained in the present work.

With reference to the present method, the main characteristics of the BEM model used to evaluate the GSIF values are the following: linear continuous boundary elements, element size far from the corner tip is 0.025h, element size at the corner tip is $10^{-8}h$ and a ratio of 1.5 between the length of consecutive elements is used for the progressive refinement along the radial edges in a neighbourhood of the corner tip. The edges converging to the corner have, respectively, 66 (θ=90º), 66 (θ=0º) and 72 (θ=-120º) elements. The deformed and undeformed shapes are shown in Fig. 8, together with a detail of the discretization at the corner tip.

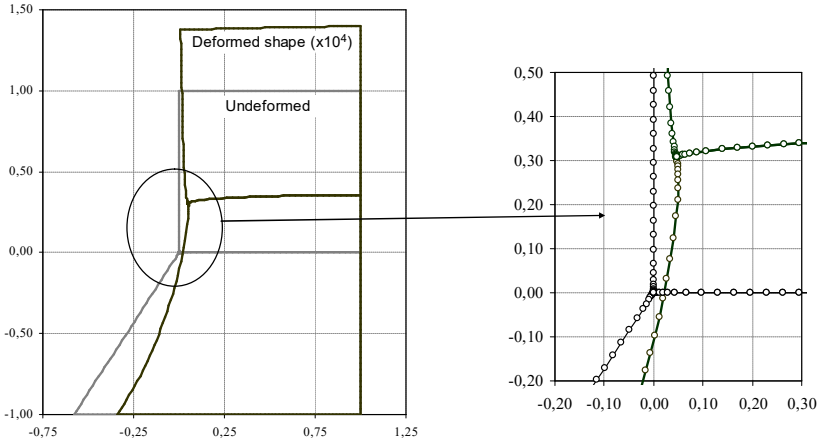

Fig. 8.- Deformed and undeformed shapes of the bimaterial problem.

Table 7 shows average values for (a_1, a_2, a_3) and their corresponding variation coefficients (in %) using in the least squares procedure the displacement components u_r and u_θ at the three edges emerging from the corner (θ= -120º, 0º and 90º), thus N_θ=3, N=66 and M=3 in equation (3). The results in each row in Table 7 correspond to all groups of nodes including the range of distances indicated. Six different ranges have been chosen to observe the influence of nodes close to the corner tip.

Unlike the values of a_1, values of a_2 and a_3 show significant variations when using nodes close to the corner tip. As soon as these nodes are excluded from the fitting procedure, the results show a clear decrease in the value of the variation coefficient, which corresponds to the flattest part of the a_i (i=1,2,3) plots.

range (mm)	a_1 (VC%)	a_2 (VC%)	a_3 (VC%)
$8.74\cdot10^{-6}$ - $4.91\cdot10^{1}$	0.678908 (1.25%)	-2.55 (>100%)	-2.64 (>100%)
$6.65\cdot10^{-5}$ - $4.91\cdot10^{1}$	0.677977 (1.08%)	-2.09 (54%)	1.50 (>100%)
$5.05\cdot10^{-4}$ - $4.91\cdot10^{1}$	0.676982 (0.92%)	-1.86 (23%)	1.14 (>100%)
$3.83\cdot10^{-3}$ - $4.91\cdot10^{1}$	0.675973 (0.77%)	-1.75979 (8.6%)	0.90 (38%)
$2.91\cdot10^{-2}$ - $3.28\cdot10^{1}$	0.675493 (0.58%)	-1.72064 (4.2%)	0.82861 (8.5%)
$1.64\cdot10^{-1}$ - $2.91\cdot10^{1}$	0.675046 (0.43%)	-1.71727 (3.9%)	0.81757 (4.5%)
selected values	0.675046	-1.71727	0.81757

Table. 7.- Results for a_1, a_2 and a_3.

Results in Table 7 show the importance of choosing an appropriate averaging area in order to correctly evaluate the values of a_i. As observed in Table 7, the number of nodes to avoid, located very close to the corner, is higher for the evaluation of a_3 than for a_2 and for a_1 respectively, as the stress singularity order is lower.

The "selected values" row appearing in Table 7 has been chosen based on results from Section 4.2, Figure 6. It shows that the results with error below 1% can be found, irrespective of the number of terms included in the asymptotic series expansion, for r_c/L ratios between 0.1 and 0.2, which is basically the choice in Table 7 (0.164-0.291).

As a first observation, see Table 8, the results from Ortiz, Alcalá and those obtained in this work are much closer (at least in a_2 and a_3) than those obtained by Qian and Akisanya. In fact, Alcalá (2008), using the explicit expressions by Qian and Akisanya, obtains results which are much more similar to those obtained using the present method than to those by Qian and Akisanya (with great differences in a_2 and a_3).

	a_1	a_2	a_3
Qian & Akisanya (1999)	0.6301	-0.3671	0.5443
Ortiz et al (2005)	0.67829	-1.54431	---
Alcalá (2008)	0.6788	-1.538	0.7732
Present work	0.675046	-1.71727	0.81757

Table. 8.- Summary of average results for a_1, a_2 and a_3.

To see the influence of using stresses and/or displacements in the procedure, data from the interface edge have been used (where both displacements and stresses are not null). A group of 25 consecutive nodes, N_r=25 in (4-5), at θ=0º in the range ($10^{-6}h<r<0.02h$) (nodes between number 10 and number 35, from a total of 66 along the edge) and M=3 has been used. Table 9 shows the results for a_1 with different combinations of displacement and stress components, making use of the appropriate values for a, b in the evaluation of (3-5).

components	a_1
u_r	0.656855 (a=1, b=0)
u_θ	0.661111 (a=1, b=0)
u_r and u_θ	0.662099 (a=1, b=0)
σ_θ	0.686260 (a=0, b=1)
$\sigma_{r\theta}$	0.634967 (a=0, b=1)
σ_θ and $\sigma_{r\theta}$	0.685272 (a=0, b=1)
u_r, u_θ, σ_θ and $\sigma_{r\theta}$	0.674215 (a=10^{12}, b=10^{-8})
u_r, u_θ and $\sigma_{r\theta}$	0.648634 (a=10^{12}, b=10^{-4})
u_r, u_θ and σ_θ	0.674305 (a=10^{12}, b=10^{-8})

Table. 9.- Results for a_1 using different displacement and stress components.

Taking the results of a_1 from Table 7 (between 0.675046 and 0.678908) for all averaging areas, results from Table 8 show that the closest result is obtained when using all displacement and stress components (u_r, u_θ, σ_θ and $\sigma_{r\theta}$) giving a value of a_1=0.674215.

To explore the capability of obtaining accurate results at a certain location using data from other locations, three different choices for the least squares fitting have been selected (Fig. 9) for the stress and displacement representation of the Qian and Akisania problem (Fig. 7) at points along a circumference with r = 0.1 h from the corner tip. The three completely different choices of nodes used in the procedure are: a) nodes along the

interface (Fig. 9a) in the range $r \leq 0.02\ h$, which represents 1/5 of the distance at which σ_{ij} and u_i will be represented in Figures 10-12, b) nodes along the interface (Fig. 9b) in the range $r \leq 0.5\ h$, five times the distance at which σ_{ij} and u_i will be represented, and c) nodes along the three edges of the problem (Fig. 9c), in the range $r \leq 0.02\ h$. All these three options use exactly the same BEM mesh, the only difference consisting in the segment of radial edges from which the BEM solution is used in the evaluation of a_i (i=1,2,3).

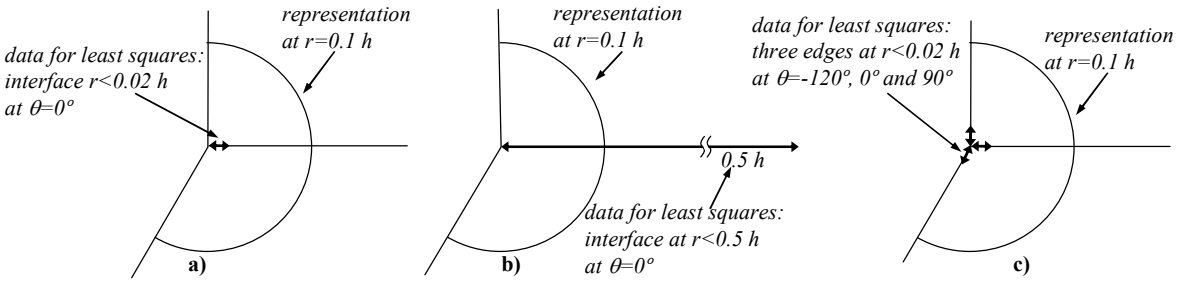

Fig. 9.- Data ranges and representations used for results in the isotropic bimaterial corner.

The displacements (u_r, u_θ) and stresses ($\sigma_{r\theta}$, σ_θ) obtained by the present procedure using the three choices defined in Fig. 9 are shown, respectively, in Figs. 10-12. In these figures, the dots represent the BEM solution at some internal points uniformly distributed along a circumference of radius r=0.1h from the corner tip, while the continuous lines are the series expressions for displacements and stresses (1) using the first three terms in addition to the rigid body rotation term.

Approximations of displacements and stresses using data from Fig. 9a and b, and shown in Fig. 10 and 11, are very good and similar in accuracy. When data from the three radial edges are included in the procedure (Fig. 9c) the comparison with the analytical solution is much better (Fig. 12) than in the two cases in which only data from one radial edge were used with data too close to and too far from the notch tip (r_c≈0.01h and r_c≈0.25h respectively, 0.1 and 2.5 times the distance from the radius r=0.1h at which σ_{ij} and u_i are represented). The procedure has shown a very robust behaviour.

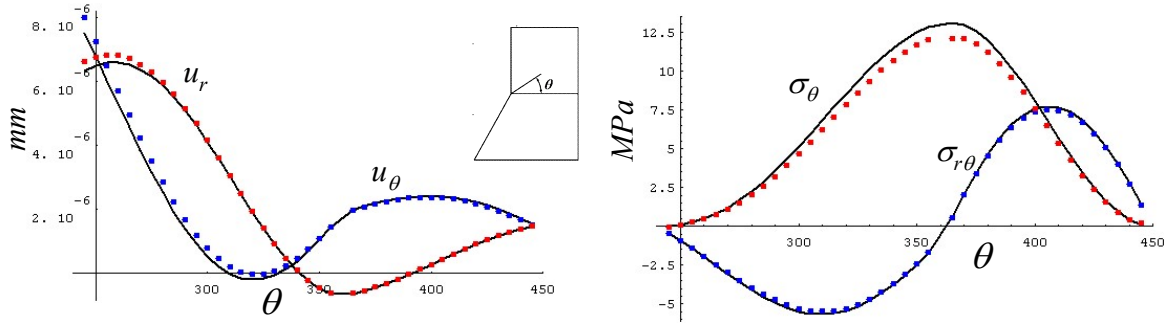

Fig. 10.- Displacements (u_r, u_θ) and stresses (σ_θ, $\sigma_{r\theta}$) at r=0.1h using displacement data from Fig.9a

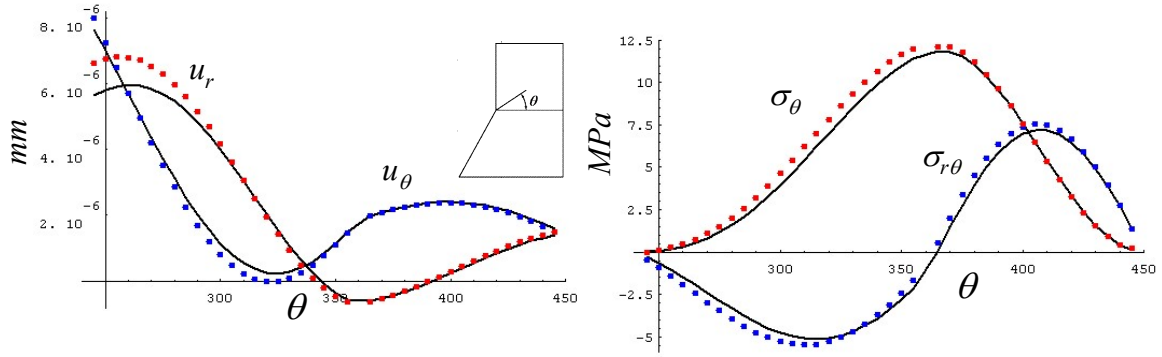

Fig. 11.- Displacements (u_r, u_θ) and stresses (σ_θ, $\sigma_{r\theta}$) at r=0.1h using displacement data from Fig.9b

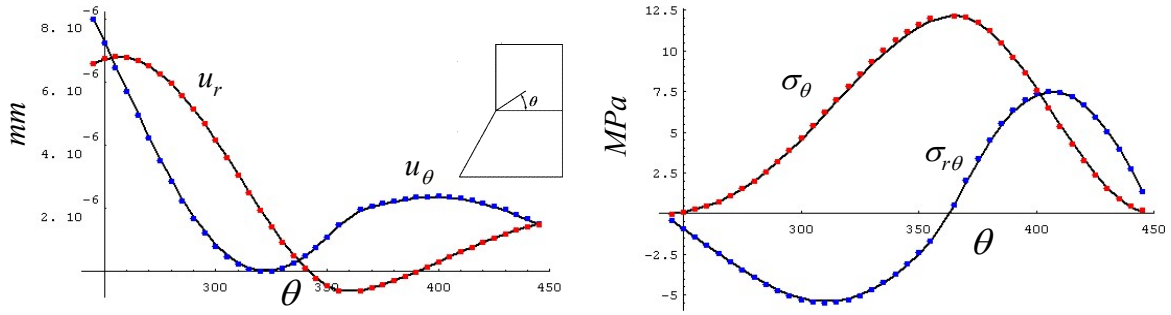

Fig. 12.- Displacements (u_r, u_θ) and stresses (σ_θ, $\sigma_{r\theta}$) at r=0.1h using displacement data from Fig.9c

The angular variation of stresses at r=0.1 h is shown in Fig.13, the dots being the BEM solution $\sigma_{\alpha\beta}^{BEM}(r,\theta)$ at internal points uniformly distributed along the circumference with radius r=0.1 h, the dashed line given by the $\sigma_{\alpha\beta}^{series}(r,\theta)$ solution for a_i (i=1,2,3) by Qian and Akisanya (1999) and the continuous line given by the present results for a_i (i=1,2,3), see Table 8. It can be seen that the stress component σ_{rr} is not continuous at the common interface (θ=0º).

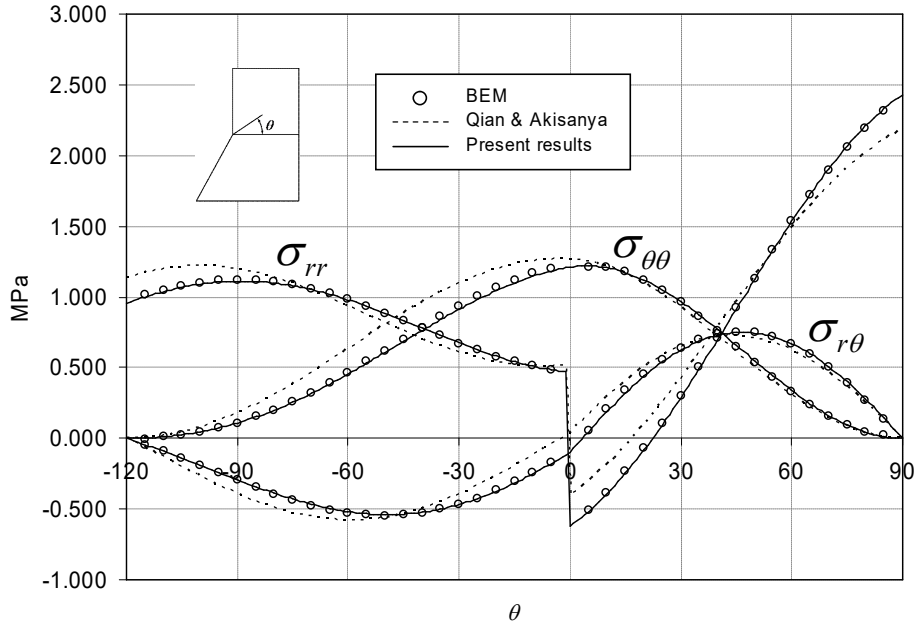

Fig. 13.- Comparison of numerical and serial stresses in the bimaterial joint at r=0.1h.

The approximation $\sigma_{\alpha\beta}^{series}(r,\theta)$ obtained using the present approach for a_i evaluation fits very well with the BEM solution $\sigma_{\alpha\beta}^{BEM}(r,\theta)$, while larger differences can be observed with the solution by Qian & Akisanya. A difference of around 7% exists in the value of a_1 between results by Qian and Akisanya and the ones obtained in the present work, while huge differences are found in a_2 and a_3 (see Table 8). These differences must nevertheless be carefully interpreted, as the characteristic angular functions for displacements (u_r, u_θ) and stresses (σ_θ, $\sigma_{r\theta}$) associated to terms 2 and 3 are quite similar, as can be observed in Fig. 14 (the modes have been conveniently multiplied for comparison purposes).

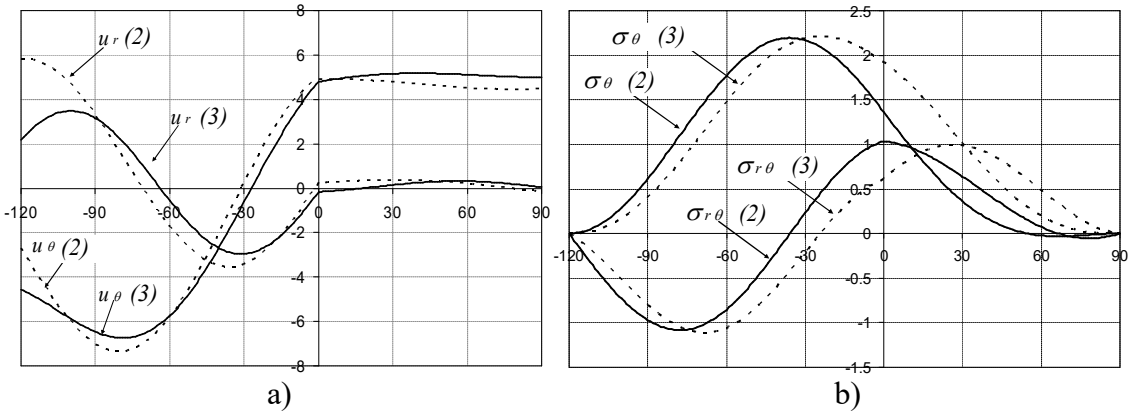

Fig. 14.- Comparison of characteristic angular functions 2 and 3 a) displacements and b) stresses.

Although, strictly speaking, the characteristic angular functions are linearly independent for different terms, if two of them are qualitatively similar in shape, as seems to be the case here (see Fig. 14), the comparison of particular values of GSIF for each term may have significant differences but the global contribution of both terms together can be quite similar. The values of a_2 and a_3 by Qian and Akisanya and those obtained in the present work are very different (Table 8), which may lead to the conclusion that one of the two results is wrong. Nevertheless, the complete stress representation in Fig. 13 does not differ as much as is indicated by the great difference in the obtained values of a_i (i=1,2,3), giving some support to the above mentioned idea. This fact can make it difficult to separate these modes and evaluate correctly the values of a_2 and a_3.

In any case, the values obtained with the present procedure, for the three a_i (i=1,2,3), are in close agreement with the results obtained by Ortiz *et al* (2005) using a different BEM code and Alcalá (2008) using explicit expressions from Qian and Akisanya, giving the impression that results obtained in the present work with the proposed procedure are reliable and can be used as a reference in this benchmark problem.

5.- Application: Singularity analysis of composite-metal adhesive lap joints

Once the present postprocessing procedure for evaluation of GSIFs has been verified in Section 4, it will be applied to a corner configuration which typically appears in structural adhesively bonded lap joints between metals and composites. In Fig. 15 a double lap joint [Aluminium (Al) (3.2 mm thickness) - Carbon Fiber Reinforced Plastic

(CFRP) $[0^o]_{12}$ (2.2 mm thickness)] is depicted. For the sake of clarity, the bimaterial corners have been conveniently magnified.

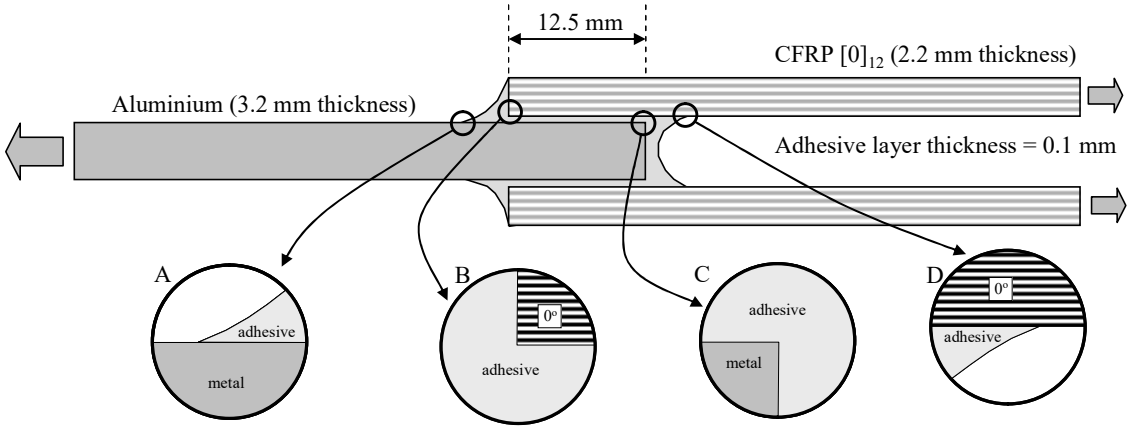

Fig. 15. Geometry of the AL-CFRP double-lap joint.

The mechanical properties of the materials are: Al (E=68.67 GPa, ν=0.33), epoxy adhesive (E=3.0, ν=0.35) and 0º CFRP (E_{11}=141.3 GPa, E_{11}=E_{22}=9.58 GPa, ν_{12}=ν_{13}=0.3, ν_{23}=0.32, G_{12}=G_{13}= 5.0 GPa, G_{23}=3.5 GPa).

Taking, for example, the inner closed corner, marked in Fig. 15 with the letter B (90º wedge of the CFRP laminate and 270º wedge of the adhesive layer and fillet), where failure typically initiates, see Barroso *et al*. (2009a), and using the tool developed by the same authors in Barroso *et al*. (2003), the following singularity exponents were obtained: λ_1=0.763236, λ_2=0.889389, λ_3=1.10698. This last one does not correspond to a singular mode as λ>1, see the stress representation in (1). Small scale yielding assumption has been verified to be valid for this case in Barroso *et al* (2009b).

The search for the GSIFs has been attempted using a BEM model and employing linear elements with a progressive refinement of the mesh towards the corner tip. The size of the smallest element adjacent to the corner is 10^{-8} mm. A uniform tensile normal stress of 125 MPa is applied at the left boundary of the aluminium plate. A detail of the joint overlap zone of the BEM model and its deformed shape are shown in Fig. 16. Only a half-part of the problem has been modelled due to the existence of symmetry.

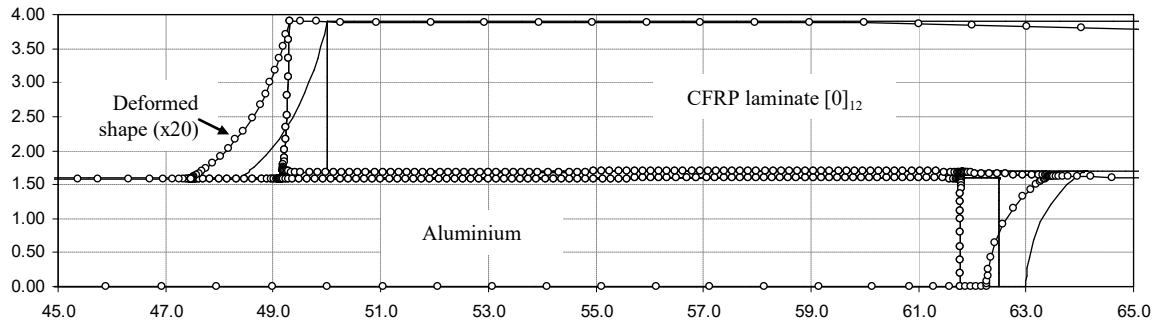

Fig. 16. BEM model (detail of the overlap zone).

The GSIF evaluation has been performed using both displacement components (u_r and u_θ) along both edges, N_θ=2 (θ_1=0º and θ_2=90º), and a coherent group of nodes between 10^{-6} mm and 0.025 mm. The nodes close to the cross point tip, where nodal displacements might be affected by the discretization, and also nodes where nodal displacements could be affected by the proximity to the boundary between adhesive and the aluminium, should be avoided. The particular values of K_m (m=1,2,3) obtained using this group of nodes fall inside the flattest zone in a K_m representation analogous to those shown in Fig. 5.

The group of nodes chosen for the evaluation of K_m (m=1,2,3) has been selected following the trends observed in Section 4.2, Figure 6. The r_c/L value of the selected group of nodes is $r_c/L\approx0.125$ which is inside the optimal range (errors below 1% irrespective of the number of terms included in the asymptotic series expansion) found in Figure 6, between 0.1 and 0.2.

The GSIF values obtained for each of the terms in the series expansion, standardized as proposed by Pageau *et al*. (1996) in such a way that the stress component $\sigma_{\theta\theta}|_{\theta=0^o}=K/(2\pi r)^{1-\lambda}$, are: K_r=-0.00356242, K_1=-0.00275036 MPa·mm$^{0.236764}$, K_2=0.0273839 MPa·mm$^{0.110611}$, K_3=-0.0114328 MPa·mm$^{-0.10698}$, the K_r term being associated to the rigid body rotation. There is evidence that failure in this type of joint is governed by values of GSIFs, see Barroso *et al* (2009).

6.- Conclusions

In the present work an efficient postprocessing procedure for the evaluation of multiple generalized stress intensity factors (GSIFs) in multimaterial corners based on BEM has been presented. The procedure is based on a simple least squares adjustment using numerical results of displacements and/or stresses along boundary edges and the common edges of the wedges in a multimaterial corner. All this makes the procedure particularly well suited for BEM codes. The procedure does not need to interact with the numerical code, and also has no special needs regarding the accuracy of results near the corner tip, where numerical errors typically may appear due to the problem discretization.

The procedure has been shown, by means of benchmark problems, to accurately evaluate the GSIFs for multiple terms in the asymptotic representation of the stress and displacement fields. The stress singularity orders and the characteristic angular functions are computed prior to the postprocessing procedure.

The procedure has proved to be robust, even in cases of multimaterial corners where only points from the material wedge interfaces (just in the radial direction) have been used to evaluate the GSIFs and these values of the GSIFs have then been used to represent the solution at a distance five times larger than the characteristic distance of the point used for the fitting procedure.

The tool has been shown to be useful in the computation of GSIFs in complicated practical situations, as is the case of an adhesively bonded double-lap joint between aluminium and a unidirectional 0º CFRP laminate.

Acknowledgments: The authors acknowledge the contribution of our ex- student Mr. Pedro Toro, who made the very first approximation to the problem, and the financial support of the Junta de Andalucía and European Social Fund through the Projects of Excellence P08-TEP-04071 and P08-TEP-04051.

References

- Alcalá, E. (2008) Characterization of elastic bimaterial corners using the Boundary Element Method (in Spanish), *Master Thesis*, University of Seville.
- Banks-Sills, L. (1997) "A conservative integral for determining stress intensity factors of a bimaterial strip". *International Journal of Fracture* **86**, 385-398.
- Barroso, A. (2007) "Characterization of singular stress states at multimaterial corners. Application to adhesively bonded joints with composite materials", PhD Thesis (in Spanish), University of Seville.
- Barroso, A., Mantič, V. and París, F. (2003) "Singularity analysis of anisotropic multimaterial corners". *International Journal of Fracture* **119**, 1-23.
- Barroso A., Toro, P., Matič, V. and París, F. (2004) "Evaluation of generalized stress intensity factors in anisotropic elastic multimaterial corners", Proceedings of the 11th European Conference on Composite Materials. Rhodes (Greece).
- Barroso A., Mantič V. and París F. (2008) "Singularity parameter determination in adhesively bonded lap joints for use in failure criteria". *Composites Science and Technology* **68**, 2671-2677.
- Barroso A., París F. and Mantič V. (2009a) "Representativity of the singular stress state in the failure of adhesively bonded joints between metals and composites". *Composites Science and Technology* **69**, 1746-1755.
- Barroso, A. Vicentini, D., Mantič, V. and París, F. (2009b) "Plasticity in bimaterial joints", *Proceedings of the COMATCOMP'09 Conference*. San Sebastián, Spain.
- Barsoum, R.S. (1976) "On the use of isoparametric finite element in linear fracture mechanics". *International Journal for Numerical Methods in Engineering* **10**, 25-37.
- Blázquez, A., Mantič, V. and París, F. (2006) "Application of BEM to generalized plane problems for anisotropic elastic materials in presence of contact". *Engineering Analysis with Boundary Elements* **30**, 489-502.
- Blázquez, A., Mantič, V., París, F. and Cañas, J. (1996) "On the removal of rigid body motions in the solution of elastostatic problems by direct BEM". *International Journal for Numerical Methods in Engineering* **39**, 4021-4038.
- Blázquez, A., París, F. and Mantič, V. (1998) "BEM solution of two-dimensional contact problems by weak application of contact conditions with non-conforming discretizations". *International Journal of Solids and Structures* **35**, 3259-3278.
- Borsuk, M. (2010) *Transmission Problems for Elliptic Second-Order Equations in Non-Smooth Domains*, Springer Basel.
- Bueckner, H.F. (1973) *Mechanics of Fracture: Methods of analysis and solution of crack problems*, G.C. Sih (Ed.), Noordhoff, Leyden, 239-314.
- Chan, S.K. Tuba, I.S. and Wilson, W.K. (1970) "On the finite element method in linear fracture mechanics". *Engineering Fracture Mechanics* **2**, 1-17.

- Cisilino, A. P. and Ortiz, J. E. (2005) “Boundary element analysis of three-dimensional mixed-mode cracks via the interaction integral”. *Computer Methods in Applied Mechanics and Engineering* **194**, 935-956.
- Costabel, M. and Dauge, M. (1993) "Construction of corner singularities for Agmon–Douglis–Niremberg elliptic systems". *Matematische Nachrichten* **162**, 209–37.
- Dempsey, J. P. and Sinclair, G. B. (1979) “On the stress singularities in the plane elasticity of the composite wedge”, *Journal of Elasticity* **9**, 373-391.
- Dempsey, J. P. and Sinclair, G. B. (1981) “On the singular behaviour at the vertex of a bi-material wedge”, *Journal of Elasticity* **11**, 317-327.
- Golub, G.H. and van Loan C.F. (1996) "Matrix computations" (Third Edition) The Johns Hopkins University Press.
- Graciani E., Mantič V., París F. and Blázquez A. (2005) "Weak formulation of axi-symmetric frictionless contact problems with boundary elements: Application to interface cracks". *Computers and Structures* **83**, 836-855.
- Gray, L. Phan, A.V., Paulino, G.H. and Kaplan, T. (2003) "Improved quarter-point crack tip element", *Engineering Fracture Mechanics* **70**, 269-283.
- Hattori, T. (1991) "A stress-singularity-parameter approach for evaluating the adhesive strength of single lap joints", *JSME International Journal*, Series I, **34**, 326-331.
- Helsing, J. and Jonsson, A. (2002a) “On the computation of stress fields on polygonal domains with V-notches”, *International Journal for Numerical Methods in Engineering* **53**, 433-453.
- Helsing, J. and Jonsson, A. (2002b) “On the accuracy of benchmark tables and graphical results in the applied mechanics literature”. *ASME Journal of Applied Mechanics* **69**, 88-90.
- Helsing, J. and Molski, K. (1996) "Elastic stress singularities and corresponding generalized stress intensity factors for angular corners under various boundary conditions", *Engineering Fracture Mechanics* **55**, 529-556.
- Henshell, R.D. and Shaw, K.G. (1975) "Crack tip finite elements are unnecessary", *Int. J. Numer. Meth. Engng.* **9**, 495-507.
- Hwu, C., Omiya, M. and Kishimoto, K. (2003) "A key matrix N for the stress singularity of the anisotropic elastic composite wedges", *JSME International Journal*, Series A **46**, 40-50.
- Hwu, C. and Kuo, T.L. (2007) "A unified definition for stress intensity factors of interface corners and cracks", *International Journal of Solids and Structures* **44**, 6340-6359.
- Knees, D. Sändig, A.-M. "Regularity of Elastic Fields in Composites", In: *Multifield Problems in Solid and Fluid Mechanics*, R. Helmig, A. Mielke, B.Wohlmuth (Eds.), Lecture Notes in Applied and Computational Mechanics, Vol. 28, p. 331-360, Springer, 2006.
- Kondratev, VA. (1967) "Boundary-value problems for elliptic equation with conical or angular points". *Trans Moscow Math Soc* **16,** 227–313.
- Liu, Y., Wu, Z., Liang, Y. and Liu, X. (2008) "Numerical methods for determination of stress intensity factors of singular stress field". *Engineering Fracture Mechanics* **75**, 4793-4803.

- Mantič, V. and París, F. (1995) "Explicit formulae of the integral kernels and C-matrix in the 2D Somigliana identity for orthotropic materials". *Engineering Analysis with Boundary Elements* **15**, 283-288.
- Mantič, V., París, F. and Cañas, J. (1997) "Stress singularities in 2D orthotropic corners". *International Journal of Fracture* **83**, 67-90.
- Mantič, V. and París, F. (1998) "Integral kernels in the 2D Somigliana displacement and stress identities for anisotropic materials". *Computational Mechanics* **22**, 77-87.
- Mantič, V. and París, F. (2004) "Advanced formulation of the BIEs for elastic anisotropic materials in 2D". Proceedings of the 5th International Conference BETEQ-04, Lisbon.
- Mantič, V., París, F. and Berger, J. (2003) "Singularities in 2D anisotropic potential problems in multi-material corners: Real variable approach". *International Journal of Solids and Structures* **40**, 5197-5218.
- Munz, D. and Yang, Y. Y. (1993) "Stresses near the edge of bonded dissimilar materials described by two stress intensity factors". *International Journal of Fracture* **60**, 169-177.
- Nomura, Y., Ikeda, T. and Miyazaki, N. (2009) "Stress intensity factor analysis at an interfacial corner between anisotropic bimaterials under thermal stress". *Engineering Fracture Mechanics* **76**, 221-235.
- Omer, N. and Yosibash, Z. (2005) "On the path independency of the point-wise J integral in three-dimensions", *International Journal of Fracture* **136**, 1-36.
- Ortiz, J., Barroso, A., Mantič, V and París, F. (2005) "Numerical characterization of 3D multimaterial corners". (in Spanish) *Proceedings of the MATCOMP-05 Conference*, 869-876, Valencia.
- Pageau, S. P., Joseph, P. F. and Biggers, Jr., S. B. (1995) "A finite element analysis of the singular stress fields in anisotropic materials loaded in antiplane shear", *International Journal for Numerical Methods in Engineering* **38**, 81-97.
- Pageau, S. P., Gadi, K. S., Biggers, Jr., S. B. and Joseph, P. F. (1996) "Standardized complex and logarithmic eigensolutions for n-material wedges and junctions". *International Journal of Fracture* **77**, 51-76.
- Paggi, M. and Carpinteri, A. (2008) "On the stress singularities at multimaterial interfaces and related analogies with fluid dynamics and diffusion", *Applied Mechanics Review* **61**.
- París, F. and Cañas, J. (1997). Boundary element method. Fundamentals and applications. Oxford: Oxford University Press.
- Qian, Z.Q. and Akisania, A.R. (1999) "Wedge corner stress behaviour of bonded dissimilar materials". *Theoretical and Applied Fracture Mechanics* **32**, 209-222.
- Quaresimin, M. and Ricotta, M. (2006) "Stress intensity factors and strain energy release rates in single lap bonded joints in composite materials". *Composites Science and Technology* **66**, 647-655.
- Sinclair, G. B., Okajima, M. y Griffin, J. H. (1984) "Path independent integrals for computing stress intensity factors at sharp corners in elastic plates". *International J. Numerical Methods in Engineering* **20**, 999-1008.
- Sinclair, G. B. (1999) "Logarithmic stress singularities resulting from various boundary conditions in angular corners of plates in extension", *Journal of Applied Mechanics* **66**, 556-559.

- Sinclair, G.B. (2004) "Stress singularities in classical elasticity-I: Removal, interpretation and analysis", *Appl. Mech. Rev.* **57**, 251-297.
- Sinclair, G.B. (2004) "Stress singularities in classical elasticity-II: Asymptotic identification", *Appl. Mech. Rev.* **57**, 385-439.
- Song, C., Tin-Loi, F. and Gao, W. (2010) "A definition and evaluation procedure of generalized stress intensity factors at cracks and multi-material wedges", *Engineering Fracture Mechanics* **77**, 2316-2336.
- Ting, T. C. T. (1997) "Stress singularities at the tip of interfaces in polycrystals", *Damage and Failure of Interfaces*, Rossmanith (ed.), Balkema, Rotterdam, 75-82.
- Trefethen, L.N. and Bau, D. *Numerical Linear Algebra*, SIAM, 1997.
- Vasilopoulos, D. (1988) "On the determination of higher order terms of singular elastic stress fields near corners", *Numerische Mathematik* **53**, 51-95.
- Wait, R. (1978) "Finite element methods for elliptic problems with singularities". *Comput. Methods Appl. Mech. Eng.* **13**, 141-150.
- Wieghardt, K. (1907) "Über das spalten und zerreissen elastischer körper", *Z Math Phys* **55**, 60–103.
- Williams, M. L. (1952) "Stress singularities resulting from various boundary conditions in angular corners of plates in extension", *Journal of Applied Mechanics* **19**, 526-528.
- Yin, W.L. (2003) "Anisotropic elasticity and multi-material singularities", *Journal of Elasticity* **71**, 263-292.